Dynamic Modeling and Parameter Identification for Cable-Driven Manipulator

Fei Yan[1], Yaoyao Wang[1], Feng Ju[1,2], Jiafeng Yao[1], Bai Chen[1], Hongtao Wu[1].

[1] College of Mechanical and Electrical Engineering, Nanjing University of Aeronautics and Astronautics, Nanjing 210016, China

[2] State Key Laboratory of Fluid Power and Mechatronic Systems, Zhejiang University, Hangzhou 310027, China

E-mail: yywang_cmee@nuaa.edu.cn (Corresponding author 1 : Dr. Wang)

E-mail: chenbye@126.com (Corresponding author 2 : Prof. Chen)

Abstract: cable-driven manipulators (CDMs) enjoy plenty of advantages, but unknown dynamic characters restrict its control performance. The motors of CDMs are put at the base and the power is transmitted by cables between motors and driving pulleys. These cables interact with the links of the manipulator, which makes the dynamic model more complicit to get. In this work, the interaction between cables and manipulators are thoroughly analyzed, and the dynamic model is derived based on Newton-Euler method. To eliminate excessive variance in recursive equations, the impact of pretension force is considered and some equivalent assumptions are proposed. To improve the accuracy of parameter identification, limited terms of Fourier series is adopted for identification trajectory. Considering various limitations of CDMs such as maximum joint angle, speed, and acceleration, artificial bee colony algorithm is used to optimize the coefficients of identification trajectory. Simulations verified that the dynamic model can precisely calculate the driving torque of CDM. Moreover, parameter identification experiment affirms the efficiency of the proposed parameter identification method.

Key Words: cable-driven manipulator, dynamics, artificial bee colony algorithm, parameter identification.

1 Introduction

Nowadays, manipulators are widely used in mass production, medical, and even, our daily lives. Traditional manipulators place their motors at their joints, which greatly increased their moving mass and inertial. Consequently, they are often isolated from human beings for sake of safety. Moreover, manipulators may suffer from malfunction due to a variety of reasons, such as program bug, mechanical abrasion and incorrect operation. Since manipulators are increasingly vital in all walks of life, it is necessary for them to be able to corporate with human or even share working space with human. Consequently, manipulators are expected to be light-weight to answer for human's safety.

Cable-driven technique is an effective tool to decrease the moving mass and rotational inertia of manipulators[1-4]. By placing motors at base and transmitting power through cables, a large amount of mass can be removed from the moving parts of manipulator [5-7]. Moreover, cable-driving spare space for other function, which makes this technique prevailing in some specific field like exoskeleton design.

There are a variety of researches dedicated to a wide range of cable-driven manipulators (CDMs). Cables bring about nonlinear friction and nonlinear motion relationship, which greatly impaired the motion accuracy of CDMs, especially when long-suspended cable is utilized. To tackle this problem, Jingli Du et al. researched into the Jacobian analysis of a long-span cable-driven manipulator. Their methods could deduce the Jacobian matrix that maps the infinitesimal change of the cable length coordinate to that of the end-effector coordinate, and could successfully find the forward solution with a very high precision[8]. Xuechao Duan et al. researched into the

calibration and motion control of a triple-level spatial positioner consisting of a 50-meter-dimensional cable-driven parallel manipulator. After kinematic calibrations, the manipulator based triple-level spatial positioner can achieve 2.55mm RMS positioning and 0.06° orientating accuracy[9]. Antonia Tzemanaki et al. designed a cable-driven mechanism as an affiliate instrument for an anthropomorphic master-slave system called μAngelo. Their design followed the utilities of the human hand, such as supination, adduction and rotation. They proposed two ways of routing the cable-driven mechanism and figured out a method to derive the input-output functions of that mechanism[10]. A. Gonzalez-Rodriguez et al. proposed a concept to improve the connection between the fixed frame and the end-effector of planar and spatial cable-driven robots. Their concept added pulleys to the attachment between the cables and the end-effector, and also included the reflective pulleys in the end-effector[11]. Renfeng Xue et al. proposed a tension-displacement transmission model for cable-pulley system to tackle nonlinear friction and backlash characteristics of cable-driven mechanism in laparoscope surgical robot. They took the bending rigidity of the cable and spatial location of the pulleys into consideration and designed a feed-forward controller using position compensation algorithm based on the model[12].

Establishing models of cable is another way to tackle the nonlinearity of cables. G. Gungor et al. researched into on-line estimation and compensation of friction in cable-driven parallel robots. They presented a recursive least-squares on-line friction estimator and an adaptive controller based on Lyapunov method[13]. Francesco Fichera et al. proposed polynomial stiffness and polynomial elastic torque model for cable-based motor-to-joint transmissions. They presented a more general elastic torque model based on polynomial stiffness, which can be applied to flexible-joint robots[14, 15]. Lingtao Yu et al. proposed a new type of wire-driven device for surgical robot, and designed an experiment model of a single joint to test the feasibility of the device. They considered the elasticity of driven cable and figured out the dynamical model of the cable-driven finger joint. They also designed an estimator of the joint angle, and modeled the DC servo motor[16]. Zhaohui Qi et al. proposed an efficient model to cope with the flexible cable with time-varying length and the coupling motions between the cable and the pulleys. Their model is useful in dynamic analysis of the cable-pulley system, but may be too complex when it comes to cable driven manipulators which use a large number of pulleys[17]. Proper trajectory is also significant for CDMs considering special nature of cables. Nan Zhang et al. proposed a geometrical approach to plan trajectories for a spatial 3-dof under-constrained cable driven parallel robot. Their approach extended beyond the static equilibrium workspace of the mechanism, and could guarantee positive and continuous tensions in cables[18]. Mourad Ismail et al. proposed a dynamic path planning algorithm for hybrid cable–serial manipulator to find the shortest and the fastest path which ensures bounded tensions in the actuators cables. They gave the trajectory through a geometric planning method, which ensures the shortest path between two poses of the robot with avoiding obstacles[19]. Many other trajectory planning methods are also valuable to CDM[20-25].

Cables bring about complicated dynamic character which challenges the control performance of CDMs. Dynamics research is worthwhile when it comes to cable-driven, so there are plenty of researches associating with it. Darwin Lau et al. considered joint interaction forces and moments in the objective functions and constraints specific to the inverse dynamics of multilink cable-driven manipulators. They formulated the relationship between the joint interactions and cable forces which included the constraints to maintain the stability of unilateral spherical joints[26]. Jingli Du et al. proposed a dynamic model for cable-driven parallel manipulators with cables of slowly time-varying length. They deduced the partial differential equation which characterized the dynamics of a cable with varying-length. They also converted the partial differential equation into ordinary differential equations

through spatial discretization by finite difference approximation[27]. Mikkel Cornelius Nielsen et al. investigated dynamics character of underwater robots. They developed a mathematical description which captured most of the significant dynamics for underwater robots[28].

Controller designation is another hotspot of CDMs. To achieve satisfactory control performance for systems under complicated uncertainties, many scholars have been devoted themselves into this filed [29-38]. Kyoungchul Kong et al. proposed a method of proxy-based impedance control as a rehabilitation algorithm of a cable-driven assistive system. They assumed free space around the proxy and a free motion of human joint is allowed in a certain range. Their methods applied assistive torque to compensate for the inertia mismatch and considered actuator dynamics for better implementation of rehabilitation algorithms[39, 40]. Since kinematic and dynamic models of cable driven parallel robots are partly structurally unknown, Reza Babaghasabha et al. proposed an adaptive robust sliding mode controller based on the adaptation of the upper bound of the uncertainties[41]. Ryan James Caverly et al. designed a state estimation for single degree of freedom flexible cable-actuated system, and used a proportional-derivative-based controller for control. They also performed estimation of the tension in each cable, and considered sensors with different sampling rates[42]. Yeongtae Jung et al. designed a cable-driven exoskeleton mechanism and addressed the problem of force control. They adopted a spring-actuator type cable-driven mechanism to make the cable routing structure compact. They design the controller by combining PD control algorithm which optimized by a linear quadratic method with a disturbance observer and feed-forward filter to track zero-phase error [43]. Quentin Boehler et al. proposed two control strategies for cable-driven tensegrity mechanism which allows us to control an angular position and the associated stiffness. The first strategy is about a tension distribution algorithm which provides a modulation of stiffness, and the second one introduces a novel velocity distribution algorithm which allows for a modulation of stiffness derivative[44]. Moreover, time delay estimation technique and sliding mode control scheme are an efficient tool in the controller design of CDM[45-51].

The model of cable-driven manipulator shown in [52] only considers joint stiffness and damping force. Multilink serial cable-driven manipulators have their cables passing through their joints, so it is inevitable that cables interact with manipulator mechanical links. In this passage, the interaction between cable and mechanical structure of manipulator will be considered and the dynamic model of cable-driven serial manipulator will be derived based on Newton-Euler method. Moreover, a parameter identification method will be proposed and proper identification trajectory will be devised. The dynamic model and parameter identification method will be verified by simulation by the collaboration of MATLAB and ADAMS software.

The contribution of this passage is as follows.

1) The dynamic model of cable-driven serial manipulator is deduced considering the interaction between cables and mechanical structure of manipulator.

2) Parameter identification method for CDM is proposed. Artificial bee colony algorithm is utilized to obtain preferred identification trajectory.

The rest of this passage is organized as follows. Section 2 describes the basic structure of cable-driven serial manipulator and deduces some preliminaries of geometry relationship. Section 3 analyzes the interaction between cables and CDMs and describes the method to obtain the dynamic model of CDM. Moreover, this section deduces the impact of pretension in cables to the dynamic model of CDM, and eliminates excessive variance in dynamic model in section 3 to make the model applicable. Section 4 describes the method for parameter identification and applies artificial bee colony algorithm to optimize the identification trajectory to achieve better identification

results. Section 5 carries out simulations to verify the dynamic model and the parameter identification method. Conclusions are drawn in section 6

2 Basic Structure and motion relationship

The basic structure of our cable-driven serial manipulator is shown in Fig.1, and the details of cable routing and guide pulley are given in Fig.2. In Fig.2, Link guide pulley is fixed to the corresponding link. The center of joint guide pulleys and joint drive pulleys are corresponding to the center of the hinges between two joints.

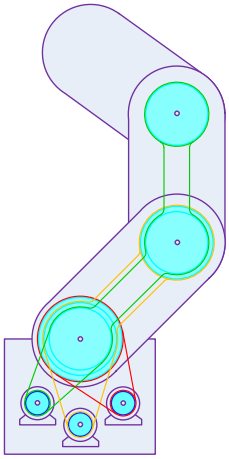

Fig.1 Basic structure of our cable-driven serial manipulator

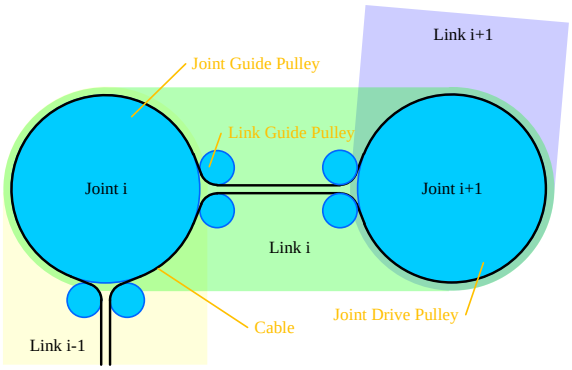

Fig.2 Details of cable routing and guide pulley

As a preliminary of dynamics to cable-driven serial manipulator, some geometry relationship will be deduced. Denote the radius of the joint guide pulley between link i-1 and link i by R. One can easily see in Fig.1 that cables passing through a joint are under length variation when the angles between links change. Specifically, if link i rotates relative to link i-1 by angle θ in anti-clockwise direction, the cable on one side wounds onto the joint guide pulley while the cable on the other side will fall from the joint guide pulley, which seems as if cable changes its length along with the rotation of links. Consequently, Link i+1 will rotates relative to link i in clockwise direction. Given that the joint guide pulleys and joint drive pulleys have the same diameter, link i+1 will rotates by angle θ, just the same as the angle that link i rotates relative to link i-1. Under this condition, link i+1 translates without rotating relative to link i-1. Notice that all the joint guide pulleys and joint drive pulleys are of equal size although they are of different size in Fig.1 for clear illustration.

Joints' extreme position of CDM is shown in Fig.3. The radius of link guide pulley is denoted by r_g; that of joint guide pulley and joint drive pulley are both r_j. The distance between the center of link guide pulleys and links'

center is d_{g0}. The line between joint guide pulley and link guide pulley is projected to coordinate axis x_i, and its length is denoted by d_{j0}. On the extreme condition shown in Fig.3, cable 1 is tangent to the joint guide pulley. At this time, the angle between two links is $2\theta_{j0}$. The meaning of extreme condition is that cable 1 will fall from joint guide pulley if link i rotates clockwise any further relative to link i-1. When cable 1 falls from joint guide pulley, motion relationship would be changed and the robot would malfunction. One can get θ_{j0} from geometry relationship shown as follows.

$$\left(\frac{r_g \cdot \sin\theta_{j0} - d_{g0}}{\cos\theta_{j0}}\right)^2 + {r_g}^2 = {d_{g0}}^2 + \left(d_{j0} - \frac{r_j}{\cos\theta_{j0}}\right)^2 \tag{1}$$

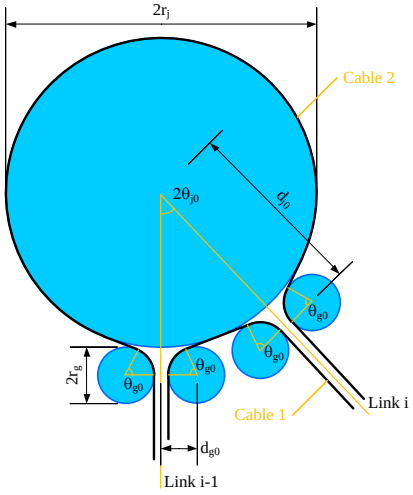

Fig.3 Joints' extreme position of CDM

It may be difficult to give an analytical solution of θ_{j0}, but a numerical solution is always available if other parameters are given. θ_{g0} is given by

$$\theta_{g0} = \frac{\pi}{2} - \theta_{j0} \tag{2}$$

Then the coordinate system will be established for dynamic analysis based on D-H method. Fig.4 shows the coordinate for link i and link i+1 without z axis which can be determine by right-hand rule. In Fig.4, the original of coordinate system for link i is located in the center of joint i where the center of the hinge between link i-1 and link i locates. The coordinate system $O_ix_iy_iz_i$, abbreviated to O_i, is fixed to link i. Link 0 denotes the base of the manipulator which is supposed to be fixed to the ground or a vehicle in uniform linear motion.

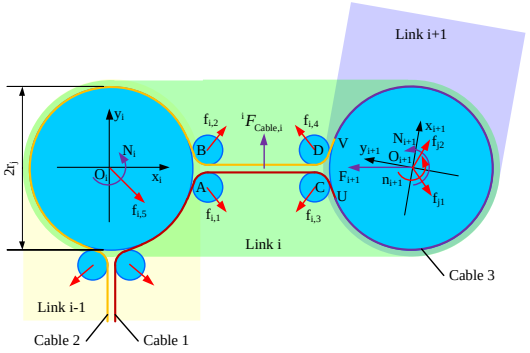

Fig.4 Coordinate for link i and link i+1

Denote ${}^{i}\omega_i$ as the rotation vector of link i relative to coordinate system i, and similarly, ${}^{i+1}\omega_{i+1}$ stands for the

rotation vector of link i+1 relative to coordinate system i+1. ${}^{i+1}_{i}\mathrm{R}$ is the transformation matrix from coordinate system O_i to O_{i+1}.

$$ {}^{i+1}_{i}\mathrm{R}=\left[{}^{i+1}\hat{\mathrm{x}}_{\mathrm{i}} \quad {}^{i+1}\hat{\mathrm{y}}_{\mathrm{i}} \quad {}^{i+1}\hat{\mathrm{z}}_{\mathrm{i}}\right]=\begin{bmatrix} \hat{\mathrm{x}}_{\mathrm{i}}\cdot\hat{\mathrm{x}}_{\mathrm{i+1}} & \hat{\mathrm{y}}_{\mathrm{i}}\cdot\hat{\mathrm{x}}_{\mathrm{i+1}} & \hat{\mathrm{z}}_{\mathrm{i}}\cdot\hat{\mathrm{x}}_{\mathrm{i+1}} \\ \hat{\mathrm{x}}_{\mathrm{i}}\cdot\hat{\mathrm{y}}_{\mathrm{i+1}} & \hat{\mathrm{y}}_{\mathrm{i}}\cdot\hat{\mathrm{y}}_{\mathrm{i+1}} & \hat{\mathrm{z}}_{\mathrm{i}}\cdot\hat{\mathrm{y}}_{\mathrm{i+1}} \\ \hat{\mathrm{x}}_{\mathrm{i}}\cdot\hat{\mathrm{z}}_{\mathrm{i+1}} & \hat{\mathrm{y}}_{\mathrm{i}}\cdot\hat{\mathrm{z}}_{\mathrm{i+1}} & \hat{\mathrm{z}}_{\mathrm{i}}\cdot\hat{\mathrm{z}}_{\mathrm{i+1}} \end{bmatrix} \tag{3} $$

$\hat{\mathrm{x}}_{\mathrm{i}}$, $\hat{\mathrm{y}}_{\mathrm{i}}$ and $\hat{\mathrm{z}}_{\mathrm{i}}$ are unit vectors to x, y and z axis, respectively. ${}^{i}_{i+1}\mathrm{R}$ gives by

$$ {}^{i}_{i+1}\mathrm{R}={}^{i+1}_{i}\mathrm{R}^{-1}={}^{i+1}_{i}\mathrm{R}^{\mathrm{T}} \tag{4} $$

The pre-superscript i+1 means they are measured in coordinate system $O_{i+1}x_{i+1}y_{i+1}z_{i+1}$. θ_i is used to describe the angle between link i-1 and link i. Specifically, θ_i is defined as

$$ \theta_{\mathrm{i}}=\arcsin\left(\left(\hat{\mathrm{x}}_{\mathrm{i-1}}\times\hat{\mathrm{x}}_{\mathrm{i}}\right)\cdot\hat{\mathrm{z}}_{\mathrm{i}}\right) \tag{5} $$

Consider that the orientation of a specific link is decided by its actuator in cable driven robot[53]. Suppose the radius of the winches of motors is r_m; q_i $\dot{q}_i$, and $\ddot{q}_i$ represents the rotation angle, speed and acceleration of the motor of link i, respectively. θ_i in eq.(5) is given by

$$ \theta_{\mathrm{i}}=\frac{r_m}{r_j}\left(q_{\mathrm{i}}-q_{\mathrm{i\text{-}1}}\right) \tag{6} $$

3 Dynamic model

Denote ${}^{\mathrm{i}}\mathrm{P}_{\mathrm{i+1}}=\overrightarrow{\mathrm{O_iO_{i+1}}}$, and ${}^{\mathrm{i}}\mathrm{P}_{\mathrm{C,i}}=\overrightarrow{\mathrm{O_iM_i}}$, where $\mathrm{M_i}$ is the mass center of link i. the pre-super script i means these vectors are measured in coordinate system O_i. ${}^{\mathrm{C,i+1}}\mathrm{I}_{\mathrm{i+1}}$ is the inertia tensor matrix of link i+1 relative to its mass center, and ${}^{\mathrm{i+1}}\dot{\mathrm{v}}_{\mathrm{C,i+1}}$ is the velocity of the mass center of link i+1. Kinematic recursion from i to i+1 are given by the following equations

$$ {}^{\mathrm{i+1}}\omega_{\mathrm{i+1}}={}^{\mathrm{i+1}}_{\mathrm{i}}R\ {}^{\mathrm{i}}\omega_{\mathrm{i}}+\dot{\theta}_{\mathrm{i}}\ {}^{\mathrm{i+1}}\hat{z}_{\mathrm{i+1}} \tag{7} $$

$$ {}^{\mathrm{i+1}}\dot{\omega}_{\mathrm{i+1}}={}^{\mathrm{i+1}}_{\mathrm{i}}R\ {}^{\mathrm{i}}\dot{\omega}_{\mathrm{i}}+{}^{\mathrm{i+1}}_{\mathrm{i}}R\ {}^{\mathrm{i}}\omega_{\mathrm{i}}\times\dot{\theta}_{\mathrm{i+1}}\ {}^{\mathrm{i+1}}\hat{z}_{\mathrm{i+1}}+\ddot{\theta}_{\mathrm{i}}\ {}^{\mathrm{i+1}}\hat{z}_{\mathrm{i+1}} \tag{8} $$

$$ {}^{\mathrm{i+1}}\dot{v}_{\mathrm{i+1}}={}^{\mathrm{i+1}}_{\mathrm{i}}R\left({}^{\mathrm{i}}\dot{\omega}_{\mathrm{i}}\times{}^{\mathrm{i}}\mathrm{P}_{\mathrm{i+1}}+{}^{\mathrm{i}}\omega_{\mathrm{i}}\times\left({}^{\mathrm{i}}\omega_{\mathrm{i}}\times{}^{\mathrm{i}}\mathrm{P}_{\mathrm{i+1}}\right)+{}^{i}\dot{v}_{i}\right) \tag{9} $$

$$ {}^{\mathrm{i+1}}\dot{\mathrm{v}}_{\mathrm{C,i+1}}={}^{\mathrm{i+1}}\dot{\omega}_{\mathrm{i+1}}\times{}^{\mathrm{i+1}}\mathrm{P}_{\mathrm{C,i+1}}+{}^{\mathrm{i+1}}\omega_{\mathrm{i+1}}\times\left({}^{\mathrm{i+1}}\omega_{\mathrm{i+1}}\times{}^{\mathrm{i+1}}\mathrm{P}_{\mathrm{C,i+1}}\right)+{}^{\mathrm{i+1}}\dot{v}_{\mathrm{i+1}} \tag{10} $$

$$ {}^{\mathrm{i+1}}F_{\mathrm{i+1}}=\mathrm{m}_{\mathrm{i+1}}\ {}^{\mathrm{i+1}}\dot{\mathrm{v}}_{\mathrm{C,i+1}} \tag{11} $$

$$ {}^{\mathrm{i+1}}N_{\mathrm{i+1}}={}^{\mathrm{C,i+1}}\mathrm{I}_{\mathrm{i+1}}\ {}^{\mathrm{i+1}}\dot{\omega}_{\mathrm{i+1}}+{}^{\mathrm{i+1}}\omega_{\mathrm{i+1}}\times{}^{\mathrm{C,i+1}}\mathrm{I}_{\mathrm{i+1}}\ {}^{\mathrm{i+1}}\omega_{\mathrm{i+1}} \tag{12} $$

Where $\mathrm{r_m}$ represents the radius of motor drive pulley. Different from traditional manipulator, cable-driven manipulators utilize cables to drive their links and place motors on their base. Apart from cables, the links are connected by hinges which provide contact force without moment. In other words, the moment of link i by link i-1 is constant zero. Thus, ${}^{\mathrm{i}}f_{\mathrm{i}}$ is used to represent the force of link i by link i-1, while ${}^{\mathrm{i}}n_{\mathrm{i}}$ is used to represent the moment of link i exerted by it driving cable which is also numbered by i. The extra force caused by cable j to link i is denoted by ${}^{i}_{j}F_{\mathrm{Cable,i}}$, and the pre-superscript means the moment is measured in coordinate system O_i. the total number of DOF is n.

$$ {}^{\mathrm{i}}f_{\mathrm{i}}={}^{\mathrm{i}}_{\mathrm{i+1}}R\ {}^{\mathrm{i+1}}f_{\mathrm{i+1}}+\sum_{j=i+1}^{n}{}^{i}_{j}F_{\mathrm{Cable,i}}+{}^{\mathrm{i}}F_{\mathrm{i}} \tag{13} $$

When cable passing through link guide pulleys, not only force ${}^{\mathrm{i}}F_{\mathrm{Cable,i}}$ is induced, but also extra moment arises. The extra moment caused by cable j to link i is denoted by ${}^{i}_{j}N_{\mathrm{Cable,i}}$, and the pre-superscript means the moment is measured in coordinate system O_i. Here number the cable which drive link i by cable i, and assume the manipulator has n degrees of freedom. To obtain ${}^{\mathrm{i}}n_{\mathrm{i}}$, sum up the moment on link i's mass center and assume the sum is zero. One can get

$$ {}^{\mathrm{i}}N_{\mathrm{i}} = {}^{\mathrm{i}}n_{\mathrm{i}} - {}^{\mathrm{i}}\mathrm{P}_{\mathrm{C,i}} \times {}^{i}f_{i} - \left({}^{\mathrm{i}}\mathrm{P}_{\mathrm{i+1}} - {}^{\mathrm{i}}\mathrm{P}_{\mathrm{C,i}}\right) \times {}^{i}f_{i+1} \tag{14} $$

where ${}^{\mathrm{i}}N_{\mathrm{i}}$ is used to represent the moment of joint i by surroundings. Consider ${}^{i}f_{i+1} = {}^{\mathrm{i}}_{\mathrm{i+1}}R^{i+1}f_{i+1}$ and substitute i in eq.(13) by i+1, one can get

$$ {}^{\mathrm{i}}n_{\mathrm{i}} = {}^{\mathrm{i}}N_{\mathrm{i}} + \sum_{j=i+1}^{n} {}^{i}_{j}N_{\mathrm{Cable,i}} + {}^{\mathrm{i}}\mathrm{P}_{\mathrm{C,i}} \times {}^{\mathrm{i}}F_{\mathrm{i}} + {}^{\mathrm{i}}\mathrm{P}_{\mathrm{i+1}} \times {}^{\mathrm{i}}_{\mathrm{i+1}}R^{i+1}f_{i+1} \tag{15} $$

Motor's driving torque is

$$ \tau_{m,\mathrm{i}} = \frac{r_m}{r_j}\hat{n}_{\mathrm{i}} \tag{16} $$

Where $\hat{n}_{\mathrm{i}}$ denote a certain element of n_i corresponding to the axis of joint. Usually, it is the third element on condition that D-H method is utilized to establish coordinate system.

In Fig.5, A segment of cable is taken for detailed analysis. A length of cable passes a joint driving pulley to drive it through friction. Consequently, the tension of that cable varies along its length that contacts the pulley. Supposing the tension changes from τ_1 to τ_2, there is a relationship between τ_1, τ_2 and n_i.

$$ n_{\mathrm{i}} = r_j\left(\tau_2 - \tau_1\right) \tag{17} $$

n_i is the torque provided by the cable to drive corresponding robot's link. Then a segment is take for further analysis. In this segment, denote the force from pulley to cable by τ_p. Denote θ as the angle that rotates from x axis to the center of this segment. θ is positive if the rotation is anti-clockwise, and is negative if the rotation direction reverses. $\vec{p}$ is the force vector from the pulley to an arbitrary point on this contact segment of the cable. θ_{p1} and θ_{p2} are the corresponding central angles of the input and output points. These angles are measured between pulley's radius and x axis, and have the same definition of positive and negative as θ. Neglecting the mass of cable and considering the force equilibrium of contact cable, the sum of force vector from the total of contact cable to the pulley can be expressed as

$$ f_{\mathrm{c}} = -\int_{\theta_{p1}}^{\theta_{p2}} p\,d\theta = \tau_1 + \tau_2 \tag{18} $$

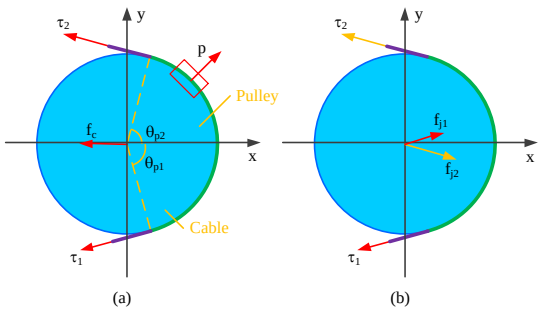

Fig.5 A segment of cable is taken for analysis

The relationship between θ_p, θ_{g0} and θ_{j0} is given by

$$\theta_{\mathrm{p}} = \frac{\pi}{2} + \theta_{\mathrm{g}0} = \pi - \theta_{j0} \tag{19}$$

Then consider the forces in Fig.4, the cable is divided into three segments, marked by Cable 1, 2, and 3, respectively. Cable 1 and 2 have constant tension; denote their tension by τ_1, and τ_2, respectively. Cable 3 has various tensions along its length. Forces between cables and links are shown by red arrows, and moment of joint drive pulley is shown by an arc with arrowhead. These forces can be expressed in coordinate system $O_i x_i y_i z_i$ as follows

$$\left[f_{i,1}, f_{i,2}, f_{i,3}, f_{i,4} \right] = \begin{bmatrix} 1-\cos\theta_{\mathrm{g}0} & 0 & 0 \\ 0 & \sin\theta_{\mathrm{g}0} & 0 \\ 0 & 0 & 1 \end{bmatrix} \begin{bmatrix} \tau_1 & \tau_2 & -\tau_1 & -\tau_2 \\ -\tau_1 & \tau_2 & -\tau_1 & \tau_2 \\ 0 & 0 & 0 & 0 \end{bmatrix} \tag{20}$$

Note that the direction of forces in Fig.4 is not necessarily the same as the direction shown in the figure; $f_{i,5}$ is given by

$$f_{i,5} = \begin{bmatrix} \cos\theta_{\mathrm{g}0}\left(\cos\theta+1\right)\left(\tau_1+\tau_2\right) + \sin\theta\sin\theta_{\mathrm{g}0}\left(\tau_2-\tau_1\right) \\ \sin\theta_{\mathrm{g}0}\left(\cos\theta-1\right)\left(\tau_2-\tau_1\right) - \sin\theta\cos\theta_{\mathrm{g}0}\left(\tau_1+\tau_2\right) \\ 0 \end{bmatrix} \tag{21}$$

Eq.(15) calculates $n_{\mathrm{i+1}}$ as driving torque for link i+1, but actually, the interact between cable and joint drive pulley is contact force and friction. Cable cannot directly provide driving torque, and consequently, the hinges between links provide a force in opposite direction of cable tensile force to form moment of couple force, shown in Fig5 (b). the moment serves as the driving torque for links instead of cable tensile force. The force provided by hinges are denoted by f_{j1} and f_{j2} corresponding to τ_1 and τ_2, respectively. Apparently, $|f_{j1}|= |\tau_1|$ and $|f_{j2}|=|\tau_2|$ holds. f_{j1} and f_{j2} are forces from link i to link i+1, so counter-acting forces are applied on link i. These counter-acting forces have the same direction and scalar as τ_1 and τ_2 with different point of action. f_{j1} and f_{j2} are given by

$$f_{j1} = \left[\tau_1\cos\theta_{\mathrm{g}0} \quad -\tau_1\sin\theta_{\mathrm{g}0} \quad 0 \right]^T \tag{22}$$

$$f_{j2} = \left[\tau_2\cos\theta_{\mathrm{g}0} \quad \tau_2\sin\theta_{\mathrm{g}0} \quad 0 \right]^T \tag{23}$$

${}^{i}_{j}F_{\mathrm{Cable,i}}$ is expressed as

$${}^{i}_{j}F_{\mathrm{Cable,i}} = \begin{cases} \sum_{k=1}^{5} {}^{i}f_{i,k} + {}^{i}f_{j1} + {}^{i}f_{j2} & , j = i+1 \\ \sum_{k=1}^{5} {}^{i}f_{i,k} & , j > i+1 \end{cases} \tag{24}$$

${}^{i}_{i+1}N_{\mathrm{Cable,i}}$ is given by

$${}^{i}_{i+1}N_{\mathrm{Cable,i}} = {}^{i}\overrightarrow{O_iA} \times {}^{i}_{j}f_{i,1} + {}^{i}\overrightarrow{O_iB} \times {}^{i}_{j}f_{i,2} + {}^{i}\overrightarrow{O_iC} \times {}^{i}_{j}f_{i,3} + {}^{i}\overrightarrow{O_iD} \times {}^{i}_{j}f_{i,4} - {}^{\mathrm{i}}\mathrm{P}_{\mathrm{i+1}} \times \left({}^{i}f_{j1} + {}^{i}f_{j2} \right) \tag{25}$$

Denote the length of link i by l_i, one can easily get

$${}^{i}\overrightarrow{O_iA} = \left[d_{j0}, -d_{g0}, 0 \right]^{\mathrm{T}} \tag{26}$$

$${}^{i}\overrightarrow{O_iB} = \left[d_{j0}, d_{g0}, 0 \right]^{\mathrm{T}} \tag{27}$$

$${}^{i}\overrightarrow{O_iC} = \left[l_i - d_{j0}, -d_{g0}, 0 \right]^{\mathrm{T}} \tag{28}$$

$${}^{i}\overrightarrow{O_iD} = \left[l_i - d_{j0}, d_{g0}, 0 \right]^{\mathrm{T}} \tag{29}$$

$${}^{i}\overrightarrow{O_iV} = \left[l_i - \mathrm{r_j}\cdot\sin\theta_{\mathrm{g}0}, \mathrm{r_j}\cdot\cos\theta_{\mathrm{g}0}, 0 \right]^{\mathrm{T}} \tag{30}$$

$$ {}^{i}\overrightarrow{O_iU} = \left[l_i - \mathrm{r_j} \cdot \sin\theta_{\mathrm{g}0}, -\mathrm{r_j} \cdot \cos\theta_{\mathrm{g}0}, 0 \right]^{\mathrm{T}} \tag{31} $$

Substitute eq.(26)-(31) into eq.(25) and simplify,

$$ {}^{i}_{i+1}N_{\mathrm{Cable,i}} = [0 \quad 0 \quad 0]^{\mathrm{T}} \tag{32} $$

On the other hand,

$$ {}^{i}_{j}N_{\mathrm{Cable,i}} = {}^{\mathrm{i}}\mathrm{P}_{\mathrm{i+1}} \times \left({}^{i}f_{j1} + {}^{i}f_{j2} \right) \quad , j > i+1 \tag{33} $$

So eq.(15) can be expressed as

$$ {}^{\mathrm{i}}n_{\mathrm{i}} = {}^{\mathrm{i}}N_{\mathrm{i}} + \sum_{j=i+2}^{n} {}^{i}_{j}N_{\mathrm{Cable,i}} + {}^{\mathrm{i}}\mathrm{P}_{\mathrm{C,i}} \times {}^{\mathrm{i}}F_{\mathrm{i}} + {}^{\mathrm{i}}\mathrm{P}_{\mathrm{i+1}} \times {}^{\mathrm{i}}_{\mathrm{i+1}}R^{i+1}f_{i+1} \tag{34} $$

Last but not least, the impact of pretension will be analyzed. Compared with traditional manipulator, cable-driven manipulators transfer power from the base to its joints by cables. It is obvious that CDMs cannot work without certain pretension, so it is necessary to figure out how the pretension influences the dynamics of CDM. Assume the manipulator has pretension τ_0 in its cables and no other force exists. In other words, assume the manipulator is isolated from other objects and free form gravity. For sake of simplicity and without loss of generality, only cable n is taken out for calculation, which is the driving cable of the distal joint of the manipulator. It can be calculated from eq.(34) that

$$ {}^{\mathrm{n}}n_{\mathrm{n}} = {}^{n}N_{n} + {}^{n}\mathrm{P}_{\mathrm{C,n}} \times {}^{n}F_{n} = \left[0 \quad 0 \quad 0\right]^{\mathrm{T}} \tag{35} $$

$$ {}^{n-1}n_{n-1} = {}^{n-1}N_{n-1} + {}^{n-1}\mathrm{P}_{\mathrm{C},n-1} \times {}^{n-1}F_{n-1} + {}^{n-1}\mathrm{P}_{n} \times {}^{n-1}_{n}R^{n} f_{n} = \left[0 \quad 0 \quad 0\right]^{\mathrm{T}} \tag{36} $$

Further, one can finally get

$$ {}^{k}n_{k} = \left[0 \quad 0 \quad 0\right]^{\mathrm{T}} \quad , \mathrm{k}=1,2,\cdots,\mathrm{n} \tag{37} $$

Actually, no matter how much pretension is exerted on cable-driven manipulator, the pretension cannot drive the manipulator. In other words, the pretension cannot act as the role of driving force, so the result of eq.(37) is easy to understand. Consequently, when deducing dynamic formula of CDMs, pretension can be subtracted from cable stress for simplification. In this passage, an assumption that $\tau_1=0$ in eq.(17) is made for simplification. Under this assumption, τ_2 is positive if it is larger than τ_1 and vice versa. Then τ_2 for joint i is expressed as

$$ \tau_{2,\,\mathrm{i}} = \frac{\mathrm{n_i}}{\mathrm{r_j}} \tag{38} $$

Eq.(20) writes

$$ \left[{}^{i}f_{i,1}, {}^{i}f_{i,2}, {}^{i}f_{i,3}, {}^{i}f_{i,4} \right] = \frac{\mathrm{n_i}}{\mathrm{r_j}} \begin{bmatrix} 0 & 1-\cos\theta_{\mathrm{g}0} & 0 & \cos\theta_{\mathrm{g}0}-1 \\ 0 & \sin\theta_{\mathrm{g}0} & 0 & \sin\theta_{\mathrm{g}0} \\ 0 & 0 & 0 & 0 \end{bmatrix} \tag{39} $$

Then eq.(24) is given by

$$ {}^{i}_{j}F_{\mathrm{Cable,i}} = \begin{cases} \dfrac{\mathrm{n_i}}{\mathrm{r_j}} \begin{bmatrix} 2\cos\theta_{\mathrm{g}0} + \cos\left(\theta - \theta_{\mathrm{g}0}\right) \\ 2\sin\theta_{\mathrm{g}0} - \sin\left(\theta - \theta_{\mathrm{g}0}\right) \\ 0 \end{bmatrix} & , j = i+1 \\ \dfrac{\mathrm{n_i}}{\mathrm{r_j}} \begin{bmatrix} \cos\theta_{\mathrm{g}0} + \cos\left(\theta - \theta_{\mathrm{g}0}\right) \\ \sin\theta_{\mathrm{g}0} - \sin\left(\theta - \theta_{\mathrm{g}0}\right) \\ 0 \end{bmatrix} & , j > i+1 \end{cases} \tag{40} $$

Finally, eq.(33) is expressed as

$$ {}^{i}_{j}N_{\text{Cable,i}} = \frac{\mathrm{n_i}}{\mathrm{r_j}} \cdot {}^{\mathrm{i}}\mathrm{P_{i+1}} \times \begin{bmatrix} \cos\theta_{\mathrm{g0}} & \sin\theta_{\mathrm{g0}} & 0 \end{bmatrix}^T \quad , j > i+1 \tag{41} $$

4 parameter identification

Last section gives the recursive method to calculate CDM's dynamics. Based on the method, one can firstly calculate ${}^{\mathrm{n}}n_{\mathrm{n}}$ and get the tension of cable n. Then ${}^{\mathrm{n-1}}n_{\mathrm{n-1}}$ can be figured out since the tension of cable n is already known. After that, ${}^{\mathrm{n-2}}n_{\mathrm{n-2}}$ is calculable as the tension of both cable n and cable n-1 is known. Step by step, all of the driving torque can be worked out and the complete dynamics model of CDM can be rearranged in matrix form shown as follows.

$$ \tau_{m,\mathrm{i}} = M\ddot{\theta}_i + C\left(\theta_i, \dot{\theta}_i\right)\dot{\theta}_i + G\left(\theta_i\right) \tag{42} $$

And eq.(42) can be further rewrite in the following form

$$ \underbrace{\tau_{m,\mathrm{i}}}_{\text{torque matrix}} = \underbrace{\begin{bmatrix} \Phi_1\left(\theta_i, \dot{\theta}_i, \ddot{\theta}_i\right) & \Phi_2\left(\theta_i, \dot{\theta}_i, \ddot{\theta}_i\right) & \cdots & \Phi_n\left(\theta_i, \dot{\theta}_i, \ddot{\theta}_i\right) \end{bmatrix}}_{\text{coefficient matrix}} \cdot \underbrace{\begin{bmatrix} P_{1,\mathrm{i}} \\ P_{2,\mathrm{i}} \\ \cdots \\ P_{n,\mathrm{i}} \end{bmatrix}}_{\text{parameter matrix}} \tag{43} $$

Where $P_{1,\mathrm{i}}, P_{2,\mathrm{i}}, \cdots, P_{n,\mathrm{i}}$ is linearly independent and is the set of the parameters to be identified for link i. It is worth to mention that different links may have the same parameters. In other words, there may be $P_{n,\mathrm{i}} = P_{m,j}$ for link i and link j. However, affecting by unknown disturbance, the result of parameter identification may differ from theoretical calculation. During parameter identification, the parameter matrix is assumed to be unknown. In other words, the aim of this procedure is to get manipulator's dynamic model without knowing manipulator's setup. Therefore, although the results obtained by parameter identification violate the relationship calculated by theory, one can accept the identification result and use it to calculate manipulator's dynamic model if the identify process is trustworthy. During experiment or simulation, a series of τ_m and θ can be gathered per time interval. Suppose a few groups of data are taken for identification; denote the total number of groups by p. Each group of data is gathered per time interval and contains a set of value consisting $\tau_m, \theta, \dot{\theta}, \ddot{\theta}$. Then the parameters to be identified can be calculated by

$$ \begin{bmatrix} P_{1,\mathrm{i}} \\ P_{2,\mathrm{i}} \\ \cdots \\ P_{n,\mathrm{i}} \end{bmatrix} = \begin{bmatrix} \Phi_{11}\left(\theta_i, \dot{\theta}_i, \ddot{\theta}_i\right) & \Phi_{21}\left(\theta_i, \dot{\theta}_i, \ddot{\theta}_i\right) & \cdots & \Phi_{n1}\left(\theta_i, \dot{\theta}_i, \ddot{\theta}_i\right) \\ \Phi_{12}\left(\theta_i, \dot{\theta}_i, \ddot{\theta}_i\right) & \Phi_{22}\left(\theta_i, \dot{\theta}_i, \ddot{\theta}_i\right) & \cdots & \Phi_{n2}\left(\theta_i, \dot{\theta}_i, \ddot{\theta}_i\right) \\ \cdots & \cdots & \cdots & \cdots \\ \Phi_{1p}\left(\theta_i, \dot{\theta}_i, \ddot{\theta}_i\right) & \Phi_{2p}\left(\theta_i, \dot{\theta}_i, \ddot{\theta}_i\right) & \cdots & \Phi_{np}\left(\theta_i, \dot{\theta}_i, \ddot{\theta}_i\right) \end{bmatrix}^{+} \begin{bmatrix} \tau_{m,\mathrm{i,1}} \\ \tau_{m,\mathrm{i,2}} \\ \cdots \\ \tau_{m,\mathrm{i,p}} \end{bmatrix} \tag{44} $$

where $\Phi_{rs}\left(\theta_i, \dot{\theta}_i, \ddot{\theta}_i\right)$ denotes $\Phi_r\left(\theta_i, \dot{\theta}_i, \ddot{\theta}_i\right)$ in data group numbered by s; $\tau_{m,\mathrm{i,s}}$ denotes $\tau_{m,\mathrm{i}}$ in data group numbered by s. $[\bullet]^+$ denote Moore-Penrose pseudo-inverse of $\bullet$. The coefficient matrix contains $\ddot{\theta}$ which is easily influenced by disturbance, so a well-designed identification trajectory for identification experiment is essential. A identification trajectory containing several terms in Fourier series is utilized and given by

$$ \hat{\theta}_d = \sum_{k=1}^{c} \hat{\mathrm{a}}_{\mathrm{k}} \cos(k\hat{w}t) + \sum_{k=1}^{c} \hat{\mathrm{b}}_{\mathrm{k}} \sin(k\hat{w}t) \tag{45} $$

where $\hat{w}$ is a positive number; c is a positive integer. These terms are restricted by the performance of

manipulator. Moreover, coefficient matrix should have small condition number which measures the sensitivity of the solution of linear equations to errors in the data. Here the condition number of a matrix is equal to the largest singular value of the matrix divided by its smallest one. Joints of manipulators have limitation in their rotation or translation ranges. Furthermore, speed and acceleration of the driving motors are limited. All of these restrictions pose limitation to the designation of identification trajectory, so eq.(45) and its derivation are restricted by the following conditions.

$$\theta_{d,\min} \le \hat{\theta}_d \le \theta_{d,\max},\ \left|\frac{\mathrm{d}}{\mathrm{dt}}\hat{\theta}_d\right| \le \omega_{d,\max},\ \left|\frac{\mathrm{d}^2}{\mathrm{dt}^2}\hat{\theta}_d\right| \le \alpha_{d,\max} \tag{46}$$

where $\theta_{d,\min}$ and $\theta_{d,\max}$ are extreme positions of rotation or those of translation of joint. $\omega_{d,\max}$ and $\alpha_{d,\max}$ are maximum joint speed and maximum joint acceleration, respectively. It is inevitable that some errors exist between desired trajectory and actual trajectory, so when determining $\theta_{d,\min}$, $\theta_{d,\max}$, $\omega_{d,\max}$ and $\alpha_{d,\max}$ margin of safety should be considered. In order to make $\hat{\theta}_d$ equal to zero at the start time, take n=c-1 and eq.(45) can be rewrite as

$$\hat{\theta}_d = \sum_{k=1}^{n} \hat{\mathrm{a}}_\mathrm{k} \cos(k\hat{w}t) + \sum_{k=1}^{n} \hat{\mathrm{b}}_\mathrm{k} \sin(k\hat{w}t) - \sum_{k=1}^{n} \hat{\mathrm{a}}_\mathrm{k} \cdot \cos(n\hat{w}t + \hat{w}t) - \sum_{k=1}^{n} \hat{\mathrm{b}}_\mathrm{k} \cdot \sin(n\hat{w}t + \hat{w}t) \tag{47}$$

moreover, eq.(47) should not take too large number as its coefficients, therefore

$$|w| \le w_{\max},\ |\hat{\mathrm{a}}_\mathrm{k}| \le a_{\max},\ \left|\hat{\mathrm{b}}_\mathrm{k}\right| \le b_{\max},\ k = 1,2,\cdots,\mathrm{n} \tag{48}$$

$$\left|\sum_{k=1}^{n} \hat{\mathrm{a}}_\mathrm{k}\right| \le a_{\max},\ \left|\sum_{k=1}^{n} \hat{\mathrm{b}}_\mathrm{k}\right| \le b_{\max},\ k = 1,2,\cdots,\mathrm{n} \tag{49}$$

Based on aforementioned restriction, artificial bee colony algorithm is utilized to calculate coefficient in eq.(47) to make the coefficient matrix in eq.(44) have as small condition number as possible. Detailed procedure of artificial bee colony algorithm is expressed in [54]. In this passage, 'food source' is a set of $\hat{\mathrm{a}}_\mathrm{k}$, $\hat{\mathrm{b}}_\mathrm{k}$, $k = 1,2,\cdots,\mathrm{n}$. When generating candidates of food source, eq.(48) acts as the upper limit and the lower limit. If the generated candidate does not satisfy the requirement of eq.(49), the algorithm will discard that and generate a new one. The objective function is the sum of two parts; one part is the condition number of coefficient matrix in eq.(43). A number much larger that the condition number of coefficient matrix will be added into objective function if the desired trajectory does not satisfy eq.(46). Thus, the other part of the objective function is zero on condition that eq.(46) is satisfied or a large number on condition that eq.(46) is violated. The fitness function can be obtained by adding 1 to objective function and calculate the reciprocal of the sum. The complete procedure to get $\hat{\mathrm{a}}_\mathrm{k}$, $\hat{\mathrm{b}}_\mathrm{k}$, $k = 1,2,\cdots,\mathrm{n}$ utilizing artificial bee colony algorithm is shown in Fig.6.

5 Numerical Example and simulation

Firstly the dynamics formula of a 2-DOF CDM is figured out utilizing aforementioned method and shown as follows.

$$\begin{aligned} n_1(3) = {} & \ddot{\theta}_1\left({}^{\mathrm{C}}\mathrm{I}_1(3,3) + \frac{1}{4}\mathrm{l}_1{}^2\mathrm{m}_1 + \mathrm{l}_1{}^2\mathrm{m}_2\right) + \frac{1}{2}\mathrm{l}_1\mathrm{l}_2\mathrm{m}_2\mathrm{c}\theta_2\left(\ddot{\theta}_1 + \ddot{\theta}_2\right) \\ & -\frac{1}{2}\mathrm{l}_1\mathrm{l}_2\mathrm{m}_2\mathrm{s}\theta_2\left(\dot{\theta}_1{}^2 + \dot{\theta}_2{}^2\right) - \dot{\theta}_1\dot{\theta}_2\mathrm{l}_1\mathrm{l}_2\mathrm{m}_2\mathrm{s}\theta_2 + g\mathrm{l}_1\mathrm{c}\theta_1\left(\frac{1}{2}\mathrm{m}_1 + \mathrm{m}_2\right) \end{aligned} \tag{50}$$

$$n_2(3)=\left(\ddot{\theta}_1+\ddot{\theta}_2\right)\left({}^{C}\mathrm{I}_2(3,3)+\frac{1}{4}\mathrm{l}_2{}^2\mathrm{m}_2\right)+\frac{1}{2}\ddot{\theta}_1\mathrm{l}_1\mathrm{l}_2\mathrm{m}_2\mathrm{c}\theta_2+\frac{1}{2}\dot{\theta}_1^2\mathrm{l}_1\mathrm{l}_2\mathrm{m}_2\mathrm{s}\theta_2+\frac{1}{2}g\mathrm{l}_2\mathrm{m}_2\mathrm{c}\theta_{12} \tag{51}$$

where $\mathrm{s}\theta_1=\sin(\theta_1)$, , $\mathrm{s}\theta_2=\sin(\theta_2)$, $\mathrm{c}\theta_2=\cos(\theta_2)$, $\mathrm{c}\theta_{12}=\cos(\theta_{12})$. $n_i(3)$ is the third element of n_i which corresponds to the driving torque of link i. similarly, ${}^{C}\mathrm{I}_1(3,3)$ denotes the element at the third row and the third column of ${}^{C}\mathrm{I}_1$. Eq.(6) and eq.(16) can be referred to $\mathrm{c}\theta_1=\cos(\theta_1)$ get the torque and rotation angle of driving motors.

Actual trajectory may differ from θ_d shown in eq.(45), so one need to use actual trajectory to modify $\hat{\mathrm{a}}_\mathrm{k}$, $\hat{\mathrm{b}}_\mathrm{k}$ and $\hat{w}$ in eq.(45). This procedure is similar as curve fitting and real trajectory can be expressed as

$$\theta=\sum_{k=1}^{n}a_\mathrm{k}\cos(kwt)+\sum_{k=1}^{n}b_\mathrm{k}\sin(kwt) \tag{52}$$

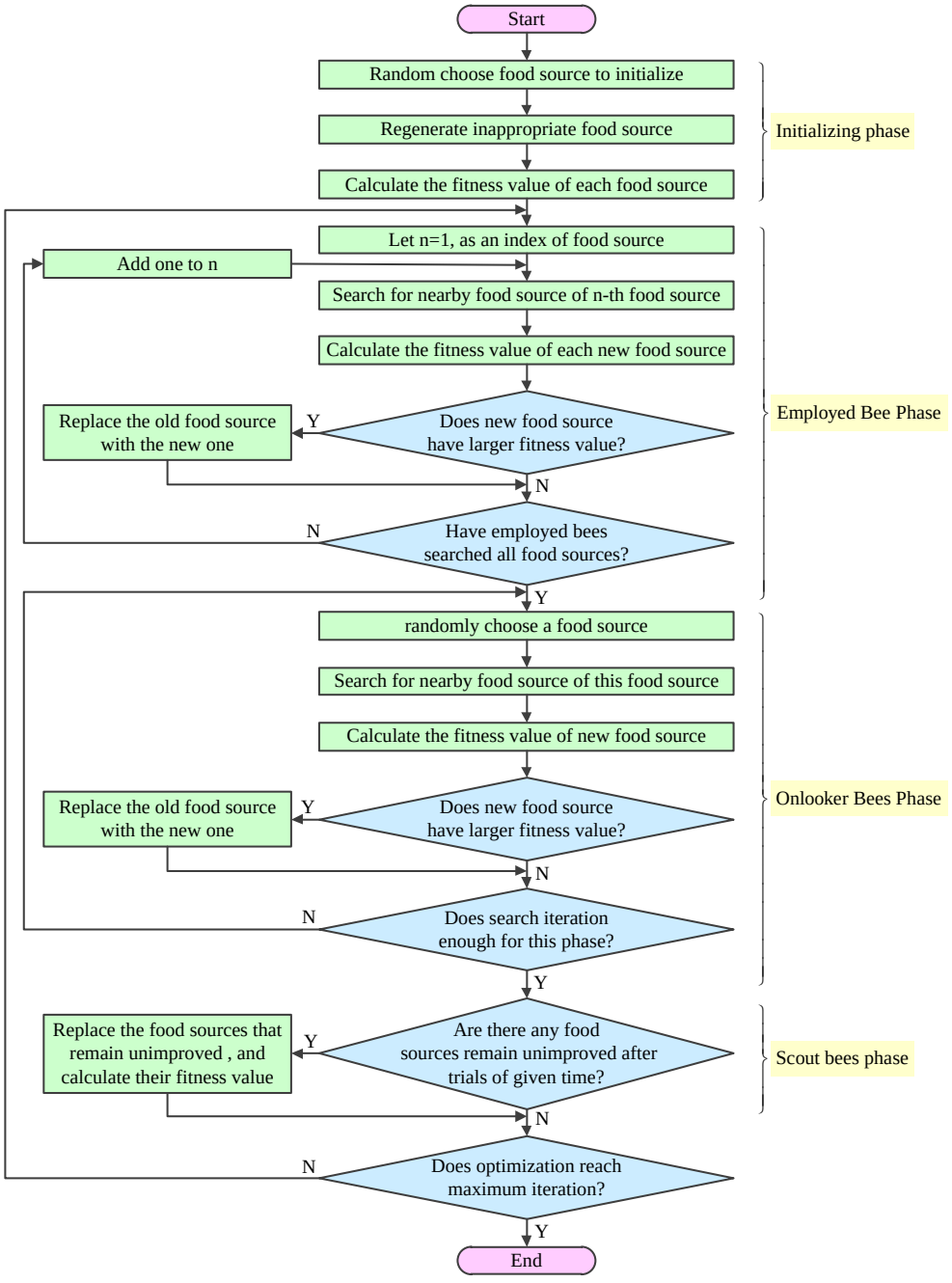

Fig.6 procedure of artificial bee colony algorithm

where w is actual moving frequency; a_k and b_k are actual coefficients for terms of Fourier series. $\dot{\theta}_i$ and $\ddot{\theta}_i$ can be obtained by take derivation of eq.(52).

A 2-DOF cable-driven manipulator is designed and simulated by ADAMS and MATLAB/Simulink. Geometry parameters of CDM are given in Table 1. θ_{g0} and θ_{j0} are calculated via eq.(1) and eq.(2) and also shown in Table 1. Links' mass center and inertia reference point are both situated at the geometry centers.

By substituting manipulator's geometry parameters into dynamic formula in section 3.1, one can get

$$\begin{aligned}\tau_{m,1} = {} & 0.6\ddot{\theta}_1 + 0.18\mathrm{c}\theta_2\left(\ddot{\theta}_1+\ddot{\theta}_2\right) - 0.18\mathrm{s}\theta_2\left(\dot{\theta}_1^2+\dot{\theta}_2^2\right) \\ & - 0.36\dot{\theta}_1\dot{\theta}_2\mathrm{s}\theta_2 + 11.76\mathrm{c}\theta_1\end{aligned} \tag{53}$$

$$\tau_{m,2} = 0.12\left(\ddot{\theta}_1+\ddot{\theta}_2\right) + 0.18\ddot{\theta}_1\mathrm{c}\theta_2 + 0.18\dot{\theta}_1^2\mathrm{s}\theta_2 + 2.94\cos\left(\theta_1+\theta_2\right) \tag{54}$$

where angles are in radians, the unit of $\tau_{m,1}$ and $\tau_{m,2}$ are $N\cdot m$.

Table 1 Geometry parameters of CDM

parameter	value	unit
l_1	0.6	meter
l_2	0.6	meter
m_1	2	kilogram
m_2	1	kilogram
d_{g0}	0.022	meter
d_{j0}	0.124	meter
r_j	0.1	meter
r_m	0.1	meter
r_g	0.02	meter
θ_{g0}	62.277	degree
θ_{j0}	27.723	degree
${}^{C}I_1$	diag(0.01,0.06,0.06)	$kg\cdot m^2$
${}^{C}I_2$	diag(0.003,0.03,0.03)	$kg\cdot m^2$

Four cases are simulated and analyzed to show the validity of the dynamic model given by eq.(53) and eq.(54).

Case 1: use sine wave as desired trajectory; only use PID controller.

Case 2: use the same desired trajectory as case 1; use PID controller with dynamic model feed-forward.

Case 3: use desired trajectory constituted by segments of quadratic polynomial; only use PID controller.

Case 4: use the same desired trajectory as case 3; use PID controller with dynamic model feed-forward.

The detailed control schemes of these cases are shown in Fig.7. In Fig.7, 'u_PID' and 'u_model' represent the control input of PID controller and dynamic model feed-forward, respectively. 'u' represents the control input that passes to the ADAMS software.

The simulation results of these cases are shown in Fig.7 and Fig.8. for sake of comparison, the control input of case 2 and case 4 are separated by two parts: one part is the control input of PID controller and the other part is the control input of dynamic model feed-forward, marked by 'PID' and 'Dynamics', respectively. One can observe that

in all of the 4 cases joints of manipulator can track desired trajectory. However, case 2 and case 4 have much less tracking error compared with case 1 and case 3, which shows the advantage of dynamic feed-forward. Moreover, when it comes to control input, the control input of dynamic model feed-forward in case 2 and case 4 is approximate to the control input of PID controller. Besides, the control input of PID controller in case 2 and case 4 is almost zero. Thus, the proposed dynamic model can precisely calculate the required control input of CDM, which proofs the validity of the proposed dynamic model.

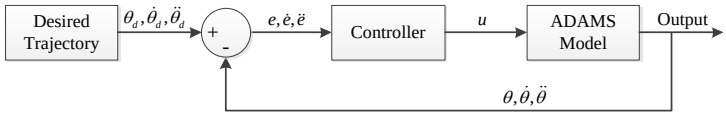

a) Control scheme of case 1 and case 3

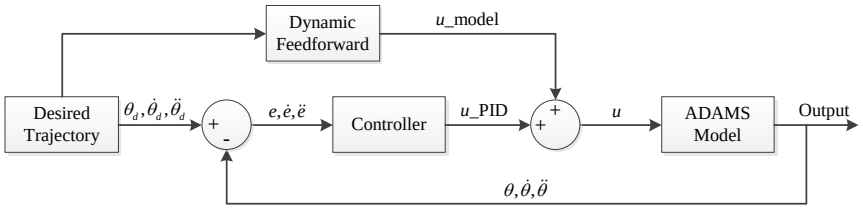

b) Control scheme of case 2 and case 4

Fig.7 Detailed control scheme of four cases

Then a parameter identification experiment of 2-DOF CDM will be carried out. The dynamic model obtained by parameter identification will be compared with the dynamic model theoretically calculated.

As a beginning of identification procedure, rewrite eq.(50) and eq.(51) as

$$\tau_{m,1}=\left[\ddot{\theta}_1 \quad \frac{1}{2}\mathrm{c}\theta_2\left(\ddot{\theta}_1+\ddot{\theta}_2\right)-\frac{1}{2}\mathrm{s}\theta_2\left(\dot{\theta}_1^2+\dot{\theta}_2^2\right)-\dot{\theta}_1\dot{\theta}_2\mathrm{s}\theta_2 \quad g\cdot\mathrm{c}\theta_1\right]\cdot\begin{bmatrix}{}^{\mathrm{C}}\mathrm{I}_1+0.25\,\mathrm{l}_1^{\,2}\mathrm{m}_1+\mathrm{l}_1^{\,2}\mathrm{m}_2\\ \mathrm{l}_1\mathrm{l}_2\mathrm{m}_2\\ \mathrm{l}_1\left(0.5\,\mathrm{m}_1+\mathrm{m}_2\right)\end{bmatrix} \tag{55}$$

$$\tau_{m,2}=\left[\ddot{\theta}_1+\ddot{\theta}_2 \quad \frac{1}{2}\ddot{\theta}_1\mathrm{c}\theta_2+\frac{1}{2}\dot{\theta}_1^2\mathrm{s}\theta_2 \quad \frac{1}{2}g\cdot\mathrm{c}\theta_{12}\right]\cdot\begin{bmatrix}{}^{\mathrm{C}}\mathrm{I}_2+0.25\,\mathrm{l}_2^{\,2}\mathrm{m}_2\\ \mathrm{l}_1\mathrm{l}_2\mathrm{m}_2\\ \mathrm{l}_2\mathrm{m}_2\end{bmatrix} \tag{56}$$

Denote

$$\begin{bmatrix}P_{1,1}\\ P_{2,1}\\ P_{3,1}\end{bmatrix}=\begin{bmatrix}{}^{\mathrm{C}}\mathrm{I}_1+0.25\,\mathrm{l}_1^{\,2}\mathrm{m}_1+\mathrm{l}_1^{\,2}\mathrm{m}_2\\ \mathrm{l}_1\mathrm{l}_2\mathrm{m}_2\\ \mathrm{l}_1\left(0.5\,\mathrm{m}_1+\mathrm{m}_2\right)\end{bmatrix} \tag{57}$$

$$\begin{bmatrix}P_{1,2}\\ P_{2,2}\\ P_{3,2}\end{bmatrix}=\begin{bmatrix}{}^{\mathrm{C}}\mathrm{I}_2+0.25\,\mathrm{l}_2^{\,2}\mathrm{m}_2\\ \mathrm{l}_1\mathrm{l}_2\mathrm{m}_2\\ \mathrm{l}_2\mathrm{m}_2\end{bmatrix} \tag{58}$$

The coefficient matrix in eq.(43) is given by

$$\begin{aligned}&\left[\Phi_1\left(\theta_1,\dot{\theta}_1,\ddot{\theta}_1\right) \quad \Phi_2\left(\theta_1,\dot{\theta}_1,\ddot{\theta}_1\right) \quad \Phi_3\left(\theta_1,\dot{\theta}_1,\ddot{\theta}_1\right)\right]=\\ &\left[\ddot{\theta}_1 \quad \frac{1}{2}\mathrm{c}\theta_2\left(\ddot{\theta}_1+\ddot{\theta}_2\right)-\frac{1}{2}\mathrm{s}\theta_2\left(\dot{\theta}_1^2+\dot{\theta}_2^2\right)-\dot{\theta}_1\dot{\theta}_2\mathrm{s}\theta_2 \quad g\cdot\mathrm{c}\theta_1\right]\end{aligned} \tag{59}$$

$$\left[\Phi_1\left(\theta_2,\dot{\theta}_2,\ddot{\theta}_2\right) \quad \Phi_2\left(\theta_2,\dot{\theta}_2,\ddot{\theta}_2\right) \quad \Phi_3\left(\theta_2,\dot{\theta}_2,\ddot{\theta}_2\right)\right]=\left[\ddot{\theta}_1+\ddot{\theta}_2 \quad \frac{1}{2}\ddot{\theta}_1\mathrm{c}\theta_2+\frac{1}{2}\dot{\theta}_1^2\mathrm{s}\theta_2 \quad \frac{1}{2}g\cdot\mathrm{c}\theta_{12}\right] \tag{60}$$

The identification trajectory is optimized by artificial bee colony algorithm and the setup of optimization is shown

in Table 2. The value of objective function during the optimization process is shown in Fig.9. The optimized identification trajectory is given as follows and a 60s segment of that is shown in Fig.10.

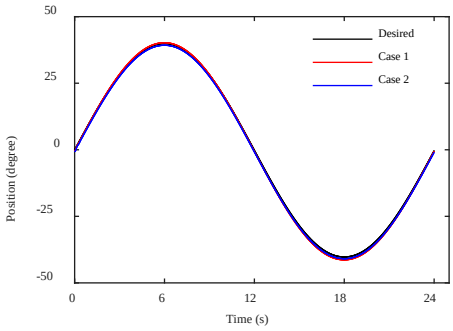

a) Position of joint 1

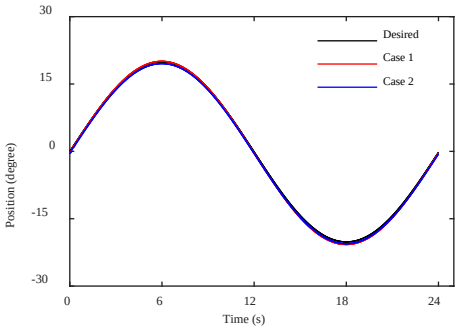

b) Position of joint 2

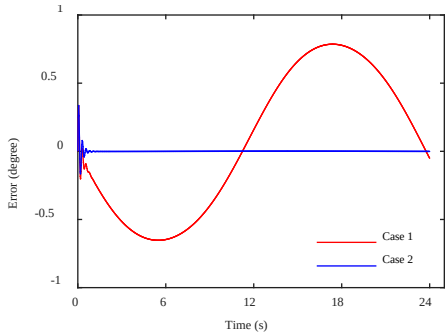

c) Tracking error of joint 1

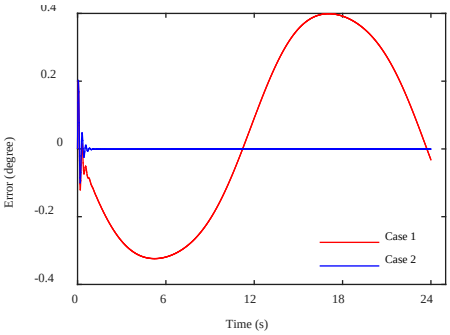

d) Tracking error of joint 2

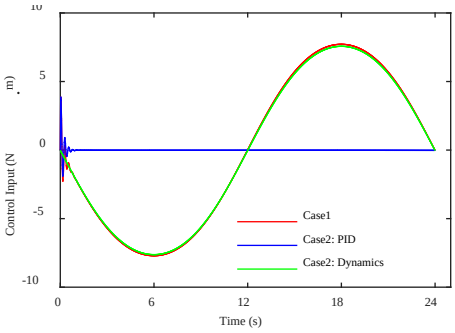

e) Control input of joint 1

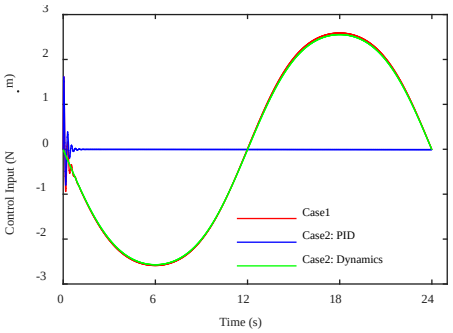

f) Control input of joint 2

Fig.8 control performance of case 1 and case 2

Table 2 the setup of optimization

Parameter	Value	Unit
$\theta_{d,\min}$, $\theta_{d,\max}$	-pi/6, pi/6	Degree
$\omega_{d,\max}$	pi/24	Degree / s
$\alpha_{d,\max}$	pi/48	Degree / s^2
$w_{\max}$	pi/6	1 / s
$a_{\max}$	1	
$b_{\max}$	1	
Number of Colony Size	20	
Number of Food Sources	10	
Maximum Number of Cycles	2000	
Number of Optimized Parameters	13	

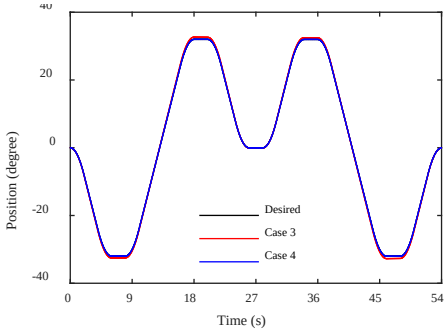

a) Position of joint 1

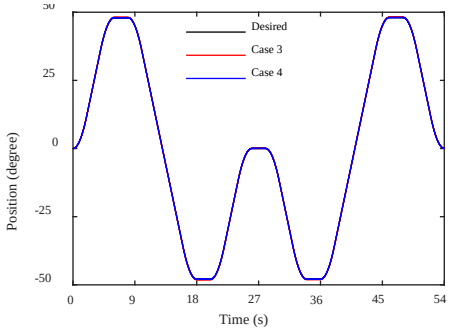

b) Position of joint 2

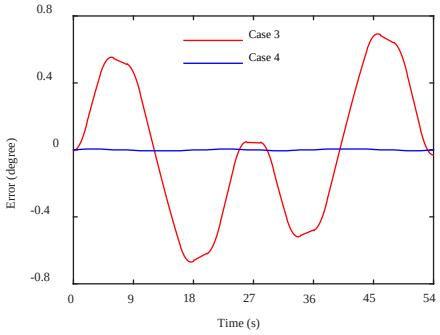

c) Tracking error of joint 1

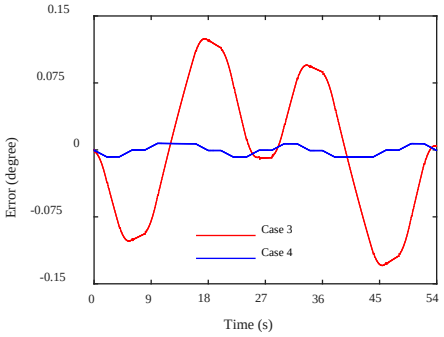

d) Tracking error of joint 2

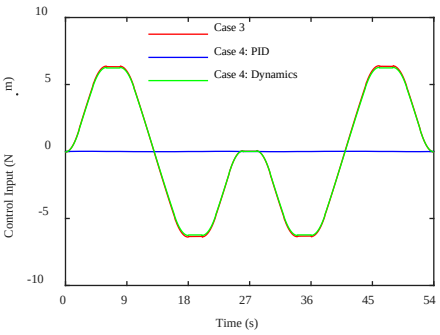

e) Control input of joint 1

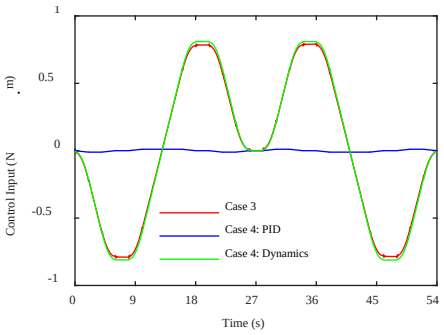

f) Control input of joint 2

Fig.9 Control performance of case 3 and case 4

$$\hat{\theta}_{d1} = 0.0174\cos(0.345t) + 0.00872\cos(0.69t) - 0.00194\cos(1.04t) - 0.0242\cos(1.38t) - 0.0114\sin(0.345t) + 0.0234\sin(0.69t) - 0.0122\sin(1.04t) + (2.0\times10^{-4})\sin(1.38t) \quad (61)$$

$$\hat{\theta}_{d2} = -0.113\cos(0.345t) + 0.0717\cos(0.69t) + 0.0146\cos(1.04t) + 0.0267\cos(1.38t) - 0.0233\sin(0.345t) - 0.0197\sin(0.69t) - 0.00164\sin(1.04t) + 0.0446\sin(1.38t) \quad (62)$$

Then a PID controller is used to control the CDM to move along the identification trajectory. The total simulation time is 300s. Considering the periodicity of identification trajectory, only 0-60s of the control input in identification experiment is show in Fig.11.

Afterwards, the actual trajectory of CDM is fitted into the form of eq.(52) and the result is given as follows

$$\hat{\theta}_{d1} = 0.0177\cos(0.345t) + 0.00893\cos(0.69t) - 0.00198\cos(1.04t) - 0.0247\cos(1.38t) - 0.0117\sin(0.345t) + 0.0239\sin(0.69t) - 0.0125\sin(1.04t) + (2.35\times10^{-4})\sin(1.38t) \quad (63)$$

$$\hat{\theta}_{d2} = -0.114\cos(0.345t) + 0.0723\cos(0.69t) + 0.0147\cos(1.04t) + 0.0267\cos(1.38t) - 0.0235\sin(0.345t) - 0.0197\sin(0.69t) - 0.00176\sin(1.04t) + 0.045\sin(1.38t) \quad (64)$$

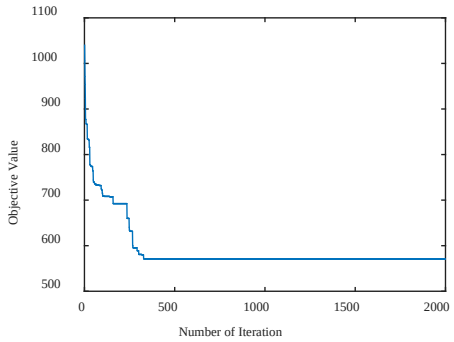

Fig.10 value of objective function during optimizing process

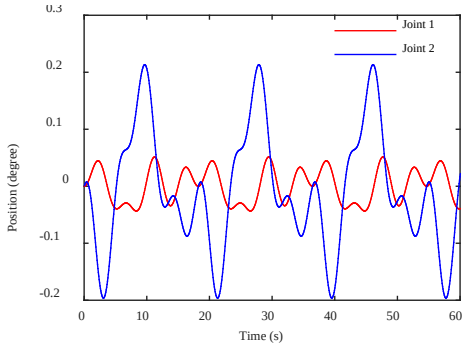

Fig.11 Optimized identification trajectory

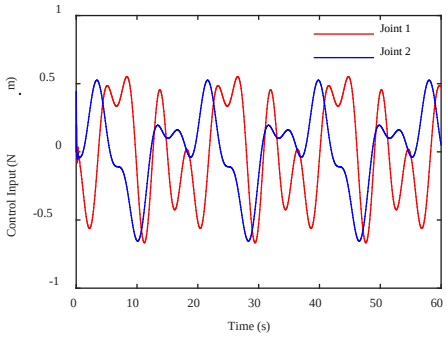

Fig.12 Control input in identification experiment

Considering that there exists relatively large tracking error at the beginning of simulation, the simulation results before 10s are discarded. 100 data points are gathered per second during simulation to form the coefficient matrix in eq.(43). Corresponding data points of control input are also recorded to form the torque matrix in eq.(43). Finally, the dynamic parameter of CDM is calculated by eq.(44) and shown as follows.

$$\begin{bmatrix} P_{1,1} & P_{2,1} & P_{3,1} \end{bmatrix} = \begin{bmatrix} 0.5997 & 0.3501 & 1.2007 \end{bmatrix}^{\mathrm{T}} \tag{65}$$

$$\begin{bmatrix} P_{1,2} & P_{2,2} & P_{3,2} \end{bmatrix} = \begin{bmatrix} 0.1195 & 0.3686 & 0.6001 \end{bmatrix}^{\mathrm{T}} \tag{66}$$

And the parameters mathematically calculated by eq.(57) and eq.(58) are given by

$$\begin{bmatrix} \hat{P}_{1,1} & \hat{P}_{2,1} & \hat{P}_{3,1} \end{bmatrix} = \begin{bmatrix} 0.6000 & 0.3600 & 1.2000 \end{bmatrix}^{\mathrm{T}} \tag{67}$$

$$\begin{bmatrix} \hat{P}_{1,2} & \hat{P}_{2,2} & \hat{P}_{3,2} \end{bmatrix} = \begin{bmatrix} 0.1200 & 0.3600 & 0.6000 \end{bmatrix}^{\mathrm{T}} \tag{68}$$

Except for the middle term of parameter matrix, the identification result is almost equal to mathematically calculated parameters. Take a look at eq.(59) and eq.(60), one may find that the middle term of coefficient matrix is rather complex. Consequently, it is difficult to get precise value of the middle term of coefficient matrix, which

will bring relatively large error to the corresponding term of parameter matrix. Therefore, generally speaking, the identification results are close to the mathematically calculated ones; the dynamic model and parameter identification method are valid.

6 Conclusion

This passage firstly describes the basic structure of CDM and deduces some geometry relationship of CDM. Then Newton-Euler recursive method is described as a basic method to obtain dynamic model of CDM. Pulleys of CDM are categorized by joint guide pulley, link guide pulley and joint drive pulley. Interaction forces between cables and these kinds of pulleys are thoroughly analyzed and figured out. To make the recursive method easy to apply, the impact of pretension in cables to dynamics is analyzed. Afterwards a parameter identification method to get dynamic model of CDM is proposed. A trajectory consist of several terms of Fourier series is used as identification trajectory to make it easier to get the acceleration of joint. In parameter identification, coefficient matrix is supposed to have as small condition number as possible. However, many restricts to identification trajectory poses challenge to obtain optimal identification trajectory. Artificial bee colony algorithm is applied to get the best identification trajectory under various restrictions. Finally, simulations verify the correctness of the proposed dynamic model and the validity of the parameter identification method.

Acknowledgements

This work was supported by the National Natural Science Foundation of China (51705243, 51575256), Natural Science Foundation of Jiangsu Province (BK20170789), and China Postdoctoral Science Foundation (2018M630552).

References

[1] Shang, W., Zhang, B., Zhang, B., et al., Synchronization control in the cable space for cable-driven parallel robots[J]. IEEE Transactions on Industrial Electronics, 2018, DOI: 10.1109/TIE.2018.2864512.

[2] Zhang, N., Shang, W. W., Cong, S., Geometry-based trajectory planning of a 3-3 cable-suspended parallel robot[J]. IEEE Trans. Robotics, 2017, 33(2), pp. 484-491.

[3] Wang, Y., Gu, L., Xu, Y., et al., Practical Tracking Control of Robot Manipulators With Continuous Fractional-Order Nonsingular Terminal Sliding Mode[J]. IEEE Transactions on Industrial Electronics, 2016, 63(10), pp. 6194-6204.

[4] Wang, Y., Yan, F., Chen, J., et al., A new adaptive time-delay control scheme for cable-driven manipulators[J]. IEEE Transactions on Industrial Informatics. DOI: 10.1109/TII.2018.2876605.

[5] Wang, Y., Li, B., Yan, F., et al., Practical adaptive fractional-order nonsingular terminal sliding mode control for a cable-driven manipulator[J]. International Journal of Robust and Nonlinear Control, 2018, DOI: 10.1002/rnc.4441.

[6] Wang, Y., Chen, J., Yan, F., et al., Adaptive super-twisting fractional-order nonsingular terminal sliding mode control of cable-driven manipulators[J]. ISA transactions, 2018, DOI: 10.1016/j.isatra.2018.11.009.

[7] Wang, Y., Jiang, S., Chen, B., et al., Trajectory Tracking Control of Underwater Vehicle-Manipulator System Using Discrete Time Delay Estimation [J]. IEEE Access, 2017, DOI: 10.1109/ACCESS.2017.2701350

[8] Du, J., Bao, H., Duan, X., et al., Jacobian analysis of a long-span cable-driven manipulator and its application to forward solution[J]. Mechanism & Machine Theory, 2010, 45(9), pp. 1227-1238.

[9] Duan, X., Qiu, Y., Duan, Q., et al., Calibration and Motion Control of a Cable-Driven Parallel Manipulator Based Triple-Level Spatial Positioner[J]. Advances in Mechanical Engineering, 2014, 6, pp. 1-10.

[10] Tzemanaki, A., Fracczak, L., Gillatt, D., et al., Design of a multi-DOF cable-driven mechanism of a miniature serial manipulator for robot-assisted minimally invasive surgery[C]. IEEE International Conference on Biomedical Robotics & Biomechatronics. IEEE, 2016, pp. 55-60.

[11] Gonzalez-Rodriguez, A., Castillo-Garcia, F. J., Ottaviano, E., et al., On the effects of the design of cable-Driven robots on kinematics and dynamics models accuracy[J]. Mechatronics, 2017, 43, pp. 18-27.

[12] Xue, R., Ren, B., Yan, Z., et al., A cable-pulley system modeling based position compensation control for a laparoscope surgical robot[J]. Mechanism and Machine Theory, 2017, 118, pp. 283-299.

[13] Gungor, G., Turhan, M. H., Jamshidifar, H., et al., Online Estimation and Compensation of Friction in Industrial Cable Robot Manipulation[J]. IFAC-PapersOnLine, 2015, 48(3), pp. 1332-1337.

[14] Grossard, M., Fichera, F., Polynomial Piece-Wise Stiffness in Cable-Based Transmissions for Robots: Modeling and Identification[J]. IFAC-PapersOnLine, 2017, 50(1), pp. 14581-14587.

[15] Fichera, F., Grossard, M., On the modeling and identification of stiffness in cable-based mechanical transmissions for robot manipulators[J]. Mechanism and Machine Theory, 2017, 108, pp. 176-190.

[16] Yu, L., Wang, W., Wang, Z., et al., Dynamical model and experimental identification of a cable-driven finger joint for surgical robot[C]. IEEE International Conference on Mechatronics & Automation. IEEE, 2017, DOI: 10.1109/ICMA.2017.8015860

[17] Qi, Z., Wang, J., Wang, G., An efficient model for dynamic analysis and simulation of cable-pulley systems with time-varying cable lengths[J]. Mechanism and Machine Theory, 2017, 116, pp. 383-403.

[18] Zhang, N., Shang, W., Dynamic trajectory planning of a 3-DOF under-constrained cable-driven parallel robot[J]. Mechanism and Machine Theory, 2016, 98, pp. 21-35.

[19] Ismail, M., Lahouar, S., Romdhane, L., Collision-free and dynamically feasible trajectory of a hybrid cable–serial robot with two passive links[J]. Robotics and Autonomous Systems, 2016, 80, pp. 24-33.

[20] Yuan, M., Chen, Z., Yao, B., et al., An Improved On-line Trajectory Planner with Stability-guaranteed Critical Test Curve Algorithm for Generalized Parametric Constraints[J]. IEEE/ASME Transactions on Mechatronics, 2018, 23(5) , pp. 2459 – 2469.

[21] Zhou, J. P., Zhong, Z. D., Wang, Z. Z., Motion Trajectory Planning of 3-Dof Wire-Driven Parallel Robot[J]. Advanced Materials Research, 2012, 424-425.

[22] Ismail, M., Samir, L., Romdhane, L., Dynamic in Path Planning of a Cable Driven Robot[M]. Design and Modeling of Mechanical Systems. 2013.

[23] Pinto, A. M., Moreira, E., José, L., et al., A cable-driven robot for architectural constructions: a visual-guided approach for motion control and path-planning[J]. Autonomous Robots, 2017, 41(7), pp. 1-13.

[24] Lahouar, S., Ottaviano, E., Zeghoul, S., et al., Collision free path-planning for cable-driven parallel robots[J]. Robotics & Autonomous Systems, 2009, 57(11) , pp. 1083-1093.

[25] Tang, L., Tang, X., Jiang, X., et al., Dynamic trajectory planning study of planar two-dof redundantly actuated cable-suspended parallel robots[J]. Mechatronics, 2015, 30, pp. 187-197.

[26] Lau, D., Oetomo, D., Halgamuge, S. K., Inverse Dynamics of Multilink Cable-Driven Manipulators with Consideration of Joint Interaction Forces and Moments[J]. IEEE Transactions on Robotics, 2015, 31(2), pp. 479-488.

[27] Xuechao, D., Yuanying, Q., Jingli, D., Dynamic Analysis and Vibration Attenuation of Cable-Driven Parallel Manipulators for Large Workspace Applications[J]. Advances in Mechanical Engineering, 2013(4) , pp. 1-6.
[28] Nielsen, M. C., Eidsvik, O. A., Blanke, M., et al., Constrained multi-body dynamics for modular underwater robots — Theory and experiments[J]. Ocean Engineering, 2018, 149, pp. 358-372.
[29] Meng, W., Yang, Q., Si, J., et al., Consensus control of nonlinear multiagent systems with time-varying state constraints[J]. IEEE transactions on cybernetics, 2017, 47(8), pp. 2110-2120.
[30] Meng, W., Yang, Q., Jagannathan, S., et al., Distributed control of high-order nonlinear input constrained multiagent systems using a backstepping-free method[J]. IEEE transactions on cybernetics, 2018, DOI: 10.1109/TCYB.2018.2853623.
[31] Yuan, M., Chen, Z., Yao, B., et al., Time optimal contouring control of industrial biaxial gantry: A highly efficient analytical solution of trajectory planning[J]. IEEE/ASME Transactions on Mechatronics, 2017, 22(1), pp. 247-257.
[32] Yuan, M., Chen, Z., Yao, B., et al., An Improved On-line Trajectory Planner with Stability-guaranteed Critical Test Curve Algorithm for Generalized Parametric Constraints[J]. IEEE/ASME Transactions on Mechatronics, 2018, 23(5), pp. 2459-2469.
[33] Deng, W., Yao, J., Ma, D., Robust adaptive precision motion control of hydraulic actuators with valve dead-zone compensation[J]. ISA Transactions, 2017, 70, pp. 269-278.
[34] Deng, W., Yao, J., Ma, D., Time-varying input delay compensation for nonlinear systems with additive disturbance: an output feedback approach[J]. International Journal of Robust and Nonlinear Control, 2018, 28(1), pp. 31-52.
[35] Chen, Z., Yao, B., Wang, Q., Accurate motion control of linear motors with adaptive robust compensation of nonlinear electromagnetic field effect[J]. IEEE/ASME Transactions on Mechatronics, 2013, 18(3), pp. 1122-1129.
[36] Chen, Z., Yao, B., Wang, Q., μ-synthesis based adaptive robust control of linear motor driven stages with high-frequency dynamics: a case study with comparative experiments[J]. IEEE/ASME Transactions on Mechatronics, 2015, 20(3), pp. 1482-1490.
[37] Chen, Z., Pan, Y. J., Gu, J., Integrated adaptive robust control for multilateral teleoperation systems under arbitrary time delays[J]. International Journal of Robust and Nonlinear Control, 2016, 26(12), pp. 2708-2728.
[38] Chen, J., Zhu, H., Zhang, L., et al., Research on fuzzy control of path tracking for underwater vehicle based on genetic algorithm optimization[J], Ocean Engineering, 2018, 156, pp. 217-223.
[39] Kong, K., Tomizuka, M., Proxy-Based Impedance Control of a Cable-Driven Assistive System for Upper Extremity Rehabilitation[J]. IFAC Proceedings Volumes, 2011, 44(1), pp. 2871-2876.
[40] Kong, K., Proxy-based impedance control of a cable-driven assistive system[J]. Mechatronics, 2013, 23(1), pp. 147-153.
[41] Babaghasabha, R., Khosravi, M. A., Taghirad, H. D., Adaptive robust control of fully-constrained cable driven parallel robots[J]. Mechatronics, 2014, 25, pp. 27-36.
[42] Caverly, R. J., Forbes, J. R., State estimator design for a single degree of freedom cable-actuated system[J]. Journal of the Franklin Institute, 2016, 353(18), pp. 4845-4869.
[43] Jung, Y., Bae, J., An asymmetric cable-driven mechanism for force control of exoskeleton systems[J]. Mechatronics, 2016, 40, pp. 41-50.

[44] Boehler, Q., Abdelaziz, S., Vedrines, M., et al., From modeling to control of a variable stiffness device based on a cable-driven tensegrity mechanism[J]. Mechanism and Machine Theory, 2017, 107, pp. 1-12.

[45] Wang, Y., Jiang, S., Chen, B., et al., A new continuous fractional-order nonsingular terminal sliding mode control for cable-driven manipulators[J]. Advances in Engineering Software, 2018, 119, pp. 21-29.

[46] Wang, Y., Yan, F., Jiang, S., et al., Time delay control of cable-driven manipulators with adaptive fractional-order nonsingular terminal sliding mode [J]. Advances in Engineering Software, 2018, 121, pp. 13-25.

[47] Wang, Y., Gu, L., Chen, B., et al., A new discrete time delay control of hydraulic manipulators [J]. Proceedings of the iMeche, Part I-Journal of Systems and Control Engineering, 2017, 231(3), pp. 168-177

[48] Wang, Y., Chen, B., Wu H., Joint space tracking control of underwater vehicle-manipulator systems using continuous nonsingular fast terminal sliding mode[J]. Proceedings of the Institution of Mechanical Engineers Part M Journal of Engineering for the Maritime Environment, 2017(9), DOI: 10.1177/1475090217742241

[49] Wang, Y., Chen, B., Wu H., Practical continuous fractional-order nonsingular terminal sliding mode control of underwater hydraulic manipulators with valve deadband compensators[J]. Proceedings of the Institution of Mechanical Engineers Part M Journal of Engineering for the Maritime Environment, 2018, DOI: 10.1177/1475090217753900

[50] Yuan, M., Chen, Z., Yao, B., et al., Time optimal contouring control of industrial biaxial gantry: A highly efficient analytical solution of trajectory planning[J]. IEEE/ASME Transactions on Mechatronics, 2017, 22(1), pp. 247-257.

[51] Deng, W., Yao, J., Ma, D., Robust adaptive precision motion control of hydraulic actuators with valve dead-zone compensation.[J]. Isa Transactions, 2017, 70, pp. 269-278.

[52] Jin, M., Lee, J., Tsagarakis, N. G., Model-free Robust Adaptive Control of Humanoid Robots with Flexible Joints[J]. IEEE Transactions on Industrial Electronics, 2017, 64(2) , pp. 1706 - 1715.

[53] Xu, W., Wang, Y., Jiang, S., et al., Kinematic analysis of a newly designed cable-driven manipulator[J]. Transactions of the Canadian Society for Mechanical Engineering, 2018, 42(2), pp. 125-135.

[54] Yan, F., Wang, Y., Xu, W., et al., Time Delay Control of Cable-Driven Manipulators with Artificial Bee Colony Algorithm[J]. Transactions of the Canadian Society for Mechanical Engineering, 2018, 42(2), pp. 177-186.